JOURNAL OF GEOPHYSICAL RESEARCH, VOL. 106, NO. D13, PAGES 14,357–14,368, JULY 16, 2001

Improving the precision of simulated hydrologic fluxes in land surface models

Jiarui Dong, Guido D. Salvucci, and Ranga B. Myneni

Department of Geography, Boston University, Boston, Massachusetts

Abstract. The numerical method for estimating soil moisture transport coefficients in land surface models (LSMs) is evaluated through comparison to a weighted-average method based on successive steady states [*Warrick*, 1991] and a proposed new scheme [*Dong and Wang*, 1997]. The focus is on situations with large gradients of soil moisture. The reference cases used to evaluate the performance of the various methods are based on numerical integrations with fine spatial resolution and small time steps. A series of tests were performed to detect sources of discrepancies and to assess the impact of various numerical methods on the simulation of evaporation, transpiration, and drainage. Off-line LSM simulations driven by observed atmospheric forcings were analyzed to understand the propagation of errors between the various hydrologic processes. We suggest a simple modification to LSM that can improve the precision of simulated hydrologic fluxes without increasing vertical resolution.

1. Introduction

Several numerical models have been developed in order to simulate the exchange of energy, mass, and momentum between the land surface and the atmosphere. Models such as the Simple Biosphere Model (SiB) [*Sellers et al.*, 1986], Biosphere-Atmosphere Transfer Scheme (BATS) [*Dickinson et al.*, 1986], the land surface model of the National Center for Atmospheric Research (NCAR-LSM) [*Bonan*, 1996], the Integrated Biosphere Simulator (IBIS) [*Foley et al.*, 1996], and the third global biome model (BIOME3) [*Haxeltine and Prentice*, 1996] describe land surface processes in terms of biophysical fluxes (latent heat, sensible heat, momentum, reflected solar radiation, and emitted longwave radiation) and biogeochemical fluxes (CO_2) that depend on the ecological and hydrological state of the land. An important component of such models is the simulation of soil water movement, which is typically accomplished with a one-dimensional, coarsely discretized numerical solution to the Richards equation. Such numerical solutions, however, can display large errors in comparison to analytical solutions of the corresponding differential equation [e.g., *Haverkamp et al.*, 1977]. The errors can be especially large under coarse spatial resolution (e.g., six layers in NCAR-LSM and IBIS) at which such models typically operate in general circulation models (GCMs). Therefore it is important to develop suitable schemes for estimating transport coefficients (soil hydraulic conductivity and diffusivity) to precisely model the distribution of soil moisture and associated fluxes.

The key to successful numerical schemes is the proper parameterization of coefficients at the interfaces between adjacent layers in the soil discretization. Previous studies have used various weighted averages. Choices for averaging the conductivity and diffusivity include arithmetic, geometric, and harmonic averages (Table 1). Results are particularly sensitive to averaging methods under conditions of large moisture gradients between adjacent layers, as occur during rainfall into dry soils. Most of the schemes result in large errors in the simulation of moisture flux because the hydraulic conductivity and diffusivity are highly nonlinear functions of soil moisture. For example, *Warrick* [1991] evaluated errors from geometrically averaged conductivity and diffusivity (case 3 of Table 1) as large as 100%, and arithmetically averaged conductivity and diffusivity (case 1 of Table 1) up to 13,321% (relative to analytical solutions under the condition of largest moisture gradient).

The land surface model in the National Center for Atmospheric Research (NCAR-LSM, version 1.0) Community Climate Model (CCM3) evaluates transport coefficients using an approximation, equal water flux across an interface (EWFAI), similar to the weighted harmonic average [*Bonan*, 1996]. The Simple Biosphere Model (SiB) uses the arithmetic weighted average of hydraulic conductivity [*Sellers et al.*, 1986], while the Integrated Biosphere Simulator (IBIS) utilizes a weighted moisture average (designated as WMA, as in case 6 in Table 1) [*Foley et al.*, 1996]. These numerical schemes can be evaluated by comparison to a benchmark calculation using a very fine spatial grid and small time step. In this paper, numerical methods used in NCAR-LSM (1.0) and IBIS were evaluated through comparison to a method developed by *Warrick* [1991] and another by *Dong and Wang* [1997], all at the same coarse resolution. Warrick's method is based on exact agreement with flow at steady state for given gradients. *Dong and Wang* [1997] developed a scheme that displayed, through comparison with field measurements, better performance than some of the weighted average methods listed in Table 1.

A series of off-line LSM experiments driven by atmospheric forcings measured at the Hydrologic Atmospheric Pilot Experiment (HAPEX) [*Goutobe and Tarrieu*, 1991] were performed to evaluate the performance, under realistic

Paper number 2001JD900126.
0148-0227/01/2001JD900126$09.00

Table 1. Numerical Schemes for Soil Hydraulic Diffusivity at an Interface

Term	Description of Methods	Formula
1	Arithmetic mean of diffusivities	$D_{i+1/2}=(D_i+D_{i+1})/2$
2	Arithmetic weighted mean of diffusivities; the weights are soil layer depth.	$D_{i+1/2}=(D_i\Delta Z_{i+1}+D_{i+1}\Delta Z_i)/(\Delta Z_i+\Delta Z_{i+1})$
3	Geometric mean of diffusivities	$D_{i+1/2}=(D_iD_{i+1})^{1/2}$
4	Harmonic mean of diffusivities	$D_{i+1/2}=2D_iD_{i+1}/(D_i+D_{i+1})$
5	Arithmetic average of moisture in two soil layers, then computation of the diffusivity	$D_{i+1/2}=D(\theta_{i+1/2})$, $\theta_{i+1/2}=(\theta_i+\theta_{i+1})/2$
6	Arithmetic weighted average of moisture in two soil layers, then computation of the diffusivity	$D_{i+1/2}=D(\theta_{i+1/2})$ $\theta_{i+1/2}=(\theta_i\Delta Z_{i+1}+\theta_{i+1}\Delta Z_i)/(\Delta Z_i+\Delta Z_{i+1})$
7	Harmonic average of moisture in two soil layers, then computation of the diffusivity	$D_{i+1/2}=D(\theta_{i+1/2})$, $\theta_{i+1/2}=2\theta_i\theta_{i+1}/(\theta_i+\theta_{i+1})$
8	Geometric average of moisture in two soil layers, then computation of the diffusivity	$D_{i+1/2}=D(\theta_{i+1/2})$, $\theta_{i+1/2}=(\theta_i\theta_{i+1})^{1/2}$
9	The minimum of moistures in two neighboring soil layers is taken to calculate diffusivity	$D_{i+1/2}=D(\min(\theta_i,\theta_{i+1}))$
10	The maximum of moistures in two neighboring soil layers is taken to calculate diffusivity	$D_{i+1/2}=D(\max(\theta_i,\theta_{i+1}))$

forcing, of the three numerical schemes on the simulation of moisture flux, evaporation, transpiration, and drainage.

2. Review of Numerical Methods

In most land surface models, flow of water through a soil column is modeled using the Darcy-Buckingham law [e.g., *Kutilek and Nielsen*, 1994]:

$$q=-\left[K(\theta)+K(\theta)\frac{\partial\psi}{\partial\theta}\frac{\partial\theta}{\partial Z}\right]=-\left[K(\theta)+D(\theta)\frac{\partial\theta}{\partial Z}\right] \quad (1)$$

In (1), q is water flux (mm s^{-1}), θ is volumetric soil moisture content (mm^3/mm^3), Z is soil depth (millimeters), t is time (seconds), $K(\theta)$ is hydraulic conductivity (mm/s), $\psi(\theta)$ is matrix potential (millimeters), and $D(\theta)$ is diffusivity (mm^2/s). The hydraulic conductivity $K(\theta)$, the soil matrix potential $\psi(\theta)$, and the hydraulic diffusivity $D(\theta)$ vary with soil moisture (θ). One common model [*Clapp and Hornberger*, 1978] used to describe this dependence is

$$K(\theta)=K_s\left(\frac{\theta}{\theta_s}\right)^{2b+3}, \quad (2)$$

$$\psi(\theta)=\psi_s\left(\frac{\theta_s}{\theta}\right)^{b}, \quad (3)$$

$$D(\theta)=K(\theta)\frac{\partial\psi(\theta)}{\partial\theta}=-\frac{K_s\psi_s b}{\theta_s}\left(\frac{\theta}{\theta_s}\right)^{b+2}. \quad (4)$$

In equations (2)-(4), K_s, ψ_s and θ_s are the hydraulic conductivity, matrix potential, and soil moisture at saturation, respectively, and b is a parameter of soil texture. All of these parameters can be related to soil texture [*Cosby et al.*, 1984].

Soil moisture movement is assumed to obey the classical Richards equation in studying the unsaturated zone [*Hillel*, 1980]. Although the θ-based Richards equation degenerates in fully saturated media, and material heterogeneity produces discontinuous θ profiles in solving groundwater hydrology problems [*Celia et al.*, 1990], most land surface models also use it to capture the diurnal, seasonal, and annual variations in soil moisture because of their practical applications and various updatings. The updatings, such as in NCAR-LSM (1.0), can prevent soil layers from becoming too wet, and also most land surface models consider only well-distributed soils and water movement under isothermal conditions. Vertical water flow in an unsaturated medium is then described by the Richards equation modified to incorporate a root sink term (S), which results from combining the Darcy-Buckingham law (1) with the continuity equation:

$$\frac{\partial\theta}{\partial t}=-\frac{\partial q}{\partial Z}-S(Z,t). \quad (5)$$

2.1. Method of Equal Water Flux Across an Interface (EWFAI)

In the NCAR-LSM (1.0) numerical solution (see Figure 1), it is assumed that the water flux from layer i (depth z_i) to the interface between layer i and layer i+1 (depth z_i+0.5Δz_i) equals the water flux from the interface to layer i+1 (depth z_{i+1}) [*Bonan*, 1996]. This flux of water (q_I) between layers i and i+1 is approximated from equation (1) as

$$q_I=-\left(\frac{2(\psi_i-\psi_{i+1})+(\Delta Z_i+\Delta Z_{i+1})}{\frac{\Delta Z_i}{K_i}+\frac{\Delta Z_{i+1}}{K_{i+1}}}\right). \quad (6)$$

Equation (6) can be rewritten as

$$q_I=-K^*\times\left(\frac{2(\psi_i-\psi_{i+1})+(\Delta Z_i+\Delta Z_{i+1})}{(\Delta Z_i+\Delta Z_{i+1})}\right), \quad (7)$$

where

$$K^*=\frac{K_iK_{i+1}}{\frac{\Delta Z_iK_{i+1}+\Delta Z_{i+1}K_i}{\Delta Z_i+\Delta Z_{i+1}}}. \quad (8)$$

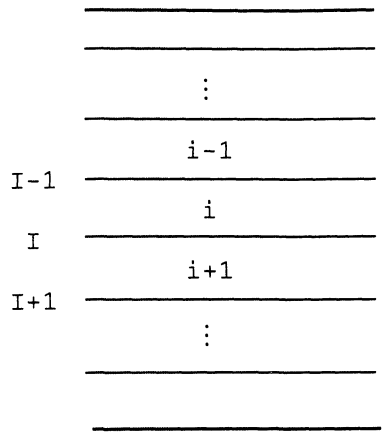

Figure 1. Soil model layers. Lowercase letters represent variables in soil layers, and capital letters denote variables at the interfaces between adjacent model layers. The layer numbers increase from surface to bottom.

This expression for K^* resembles a weighted harmonic average (reference to term 4 in Table 1). The performance of this method will be investigated in the following section.

Using a finite difference approximation with an explicit scheme in time and adding a sink term for root moisture extraction, equation (5) at layer i (Figure 1) can be written as

$$\frac{\theta_i^{n+1}-\theta_i^n}{\Delta t}=\frac{1}{\Delta Z_i}[q_I-q_{I-1}]-s_i\,. \tag{9}$$

In (9) the symbol n denotes time increment, q_I is the water flux at the interface between adjacent layers i-1 and i, and s_i is the sink of moisture due to transpiration (and soil evaporation in the surface layer). NCAR-LSM (1.0) further assumes that the water flux q_I can be expressed as

$$q_I=q_I^n+\frac{\partial q_I}{\partial\theta_i}\Delta\theta_i+\frac{\partial q_I}{\partial\theta_{i+1}}\Delta\theta_{i+1}\,, \tag{10}$$

where q_I^n is the water flux evaluated at the beginning of the time step. From equations (10) and (9), a tridiagonal system of equations for $\Delta\theta$ results:

$$S_i+q_{I-1}^n-q_I^n=-\left[\frac{\partial q_{I-1}}{\partial\theta_{i-1}}\right]\Delta\theta_{i-1}+\left[\frac{\partial q_I}{\partial\theta_i}-\frac{\partial q_{I-1}}{\partial\theta_i}-\frac{\Delta Z_i}{\Delta t}\right]\Delta\theta_i+\left[\frac{\partial q_I}{\partial\theta_{i+1}}\right]\Delta\theta_{i+1}\,. \tag{11}$$

S_i is equal to $s_i\Delta Z_i$. Equation (11) can be solved to obtain the $\Delta\theta_i$ through forward and backward iterative computation for the boundary conditions $q_{I-1}=-q_{\text{infl}}$ at the first layer (I=1) and $q_I=-K(\theta_i)$ at the bottom layer. Here, q_{infl} is defined as the flux of water into the soil, positive upward.

2.2. Method of Warrick

A weighted average of conductivity can be defined by approximating the flux as spatially constant in one layer during one time interval, such that the steady state method of *Warrick* [1991] can be applied. Thus flux at the interface, q_I, can be approximated as

$$q_I=-\left((K_w)_I+(D_w)_I\frac{\partial\theta}{\partial Z}\right), \tag{12}$$

where the weighted conductivity and diffusivity are

$$(K_w)_I=wK(\theta_i)+(1-w)K(\theta_{i+1})\,, \tag{13}$$

$$(D_w)_I=wD(\theta_i)+(1-w)D(\theta_{i+1})\,. \tag{14}$$

In (13) and (14) the weight w is obtained from the lookup table (LUT) for given gradients.

Equation (12) is integrated over the layer, with the thickness of soil layer selected as the dependent variable,

$$\Delta x=-\int_\theta^{\theta+\Delta\theta}\frac{D(\theta')}{q+K(\theta')}d\theta'\,. \tag{15}$$

In (15) the moisture flux q can be written as

$$q=w\left\{K(\theta+\Delta\theta)-K(\theta)+[D(\theta+\Delta\theta)-D(\theta)]\frac{\Delta\theta}{\Delta x}\right\}-\left\{K(\theta+\Delta\theta)+D(\theta+\Delta\theta)\frac{\Delta\theta}{\Delta x}\right\}. \tag{16}$$

The conductivity $K(\theta)$ and diffusivity $D(\theta)$ are nonlinear functions of soil moisture, and therefore no analytical solution of equation (15) can be found. However, a lookup table for weights can be obtained based on numerical analysis. Convergence can be attained and verified by a separate integration using a second-order Simpson algorithm with a tolerance of 10^{-5}. To do this, let

$$f(x)=-\frac{D(x)}{q+K(x)}\,,$$

$$\int_{x_1}^{x_3}f(x)dx=h[\frac{1}{3}f_1+\frac{4}{3}f_2+\frac{1}{3}f_3]\,,$$

where $x_1=\theta+kh$, $x_3=x_1+2h$, and h is defined as the increment used in the second order Simpson algorithm. The parameter k takes values of 0, 2, 4, ..., N-2 for each given gradient of soil moisture, and $N=\Delta\theta/h$. Here, both θ and $\theta+\Delta\theta$ take values of 0.01, 0.1, 0.2, 0.3, 0.4, and 0.435 (mm^3/mm^3) for a specific soil. Similarly, the thickness Δz is taken as 10 mm for the fine-resolution calculations, and 150, 300, 600, 1200, and 2400 mm for the coarse-resolution experiments. The corresponding tables of weights are thus constructed. For any θ and $\theta+\Delta\theta$, the corresponding weight can be obtained through bilinear interpolation of weights in the LUT. The soil moisture profile is then simulated by substituting equations (12), (13), and (14) into a tridiagonal system of equations (11) for specific boundary and initial conditions.

2.3. Method of Dong and Wang

In this method the hydraulic conductivity and diffusivity are determined at two different interpolated moisture contents ($\theta_I^{(K)}$ and $\theta_I^{(D)}$, respectively) at the interface between model layers as power-weighted averages of moisture in the two surrounding layers [*Dong and Wang*, 1997]. The water flux q_I is thus given as

$$q_I=-\left(K(\theta)+D(\theta)\frac{\partial\theta}{\partial Z}\right)_I$$

$$= -\left(K(\theta_I^{(K)}) + D(\theta_I^{(D)}) \frac{\theta_i - \theta_{i+1}}{(\Delta Z_i + \Delta Z_{i+1})/2} \right). \quad (17)$$

To derive $\theta_I^{(K)}$ and $\theta_I^{(D)}$, note that the two terms $\partial K(\theta)/\partial Z$ and $D(\theta)\partial\theta/\partial Z$ from equations (1) and (5) can be written in the common form $\partial A\theta^B/\partial Z$. By applying the Clapp and Hornberger relations, for $\partial K(\theta)/\partial Z$, $A=K_s/\theta_s^{2b+3}$ and $B=2b+3$, while for $D(\theta)\partial\theta/\partial Z$, $A=K_s\psi_s b/(b+3)\theta_s^{b+3}$ and $B=b+3$. Finite-differencing these transformed derivatives then implies that the interpolated soil moisture at the interface I between layers i-1 and i can be expressed [*Dong and Wang*, 1997] for conductivity evaluation ($\theta_I^{(K)}$) and diffusivity evaluation ($\theta_I^{(D)}$) as

$$\theta_I^{(K)} = \left(\frac{\theta_i^{2b+3} - \theta_{i+1}^{2b+3}}{(2b+3)(\theta_i - \theta_{i+1})} \right)^{\frac{1}{2b+2}}, \quad (18)$$

$$\theta_I^{(D)} = \left(\frac{\theta_i^{b+3} - \theta_{i+1}^{b+3}}{(b+3)(\theta_i - \theta_{i+1})} \right)^{\frac{1}{b+2}}. \quad (19)$$

Equation (11), together with equations (18) and (19), forms the basis of this method.

3. Numerical Simulation With the EWFAI Method

The EWFAI, the numerical scheme for soil water flux simulation in NCAR-LSM (1.0), was used to perform a series of simulations with different initial and boundary conditions. The soil hydraulic properties are those reported in NCAR-LSM (1.0) and the work by *Cosby et al.* [1984], and they vary based on soil texture. The soil column is divided into six layers of thickness 100, 200, 400, 800, 1600, and 3200 mm. All variables (i.e., soil moisture (θ_i), hydraulic conductivity (K_i), matrix potential (ψ_i), and hydraulic diffusivity (D_i)) are defined at the center of each layer. The soil in these calculations is a loamy soil, with 43% sand, 18% clay, and 39% loam. The following typical values of the soil parameters are used: K_s= 0.0042 mm/s, θ_s= 0.435 mm^3/mm^3, ψ_s= −207 mm, and b = 5.77.

After applying equation (11), NCAR-LSM (1.0) updates the soil moisture profile at each time step according to the

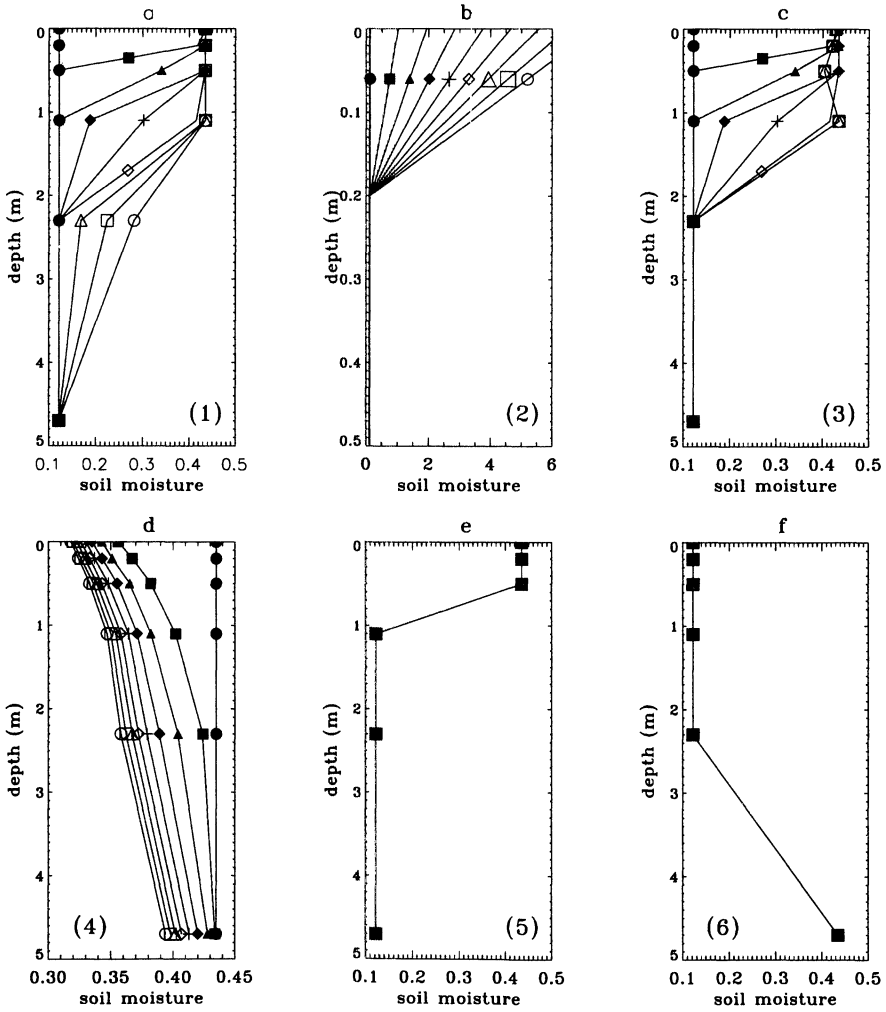

Figure 2. Soil moisture profiles simulated with the numerical method from NCAR LSM (version 1.0) under different initial and boundary conditions (listed in Table 2). Cases 1, 2, and 3 show simulations of infiltration, cases 4 and 5 test the drainage modeling, and case 6 tests the moisture exfiltration from bottom layer. The symbols denote the moisture profiles at the start (solid circles) and at 6-hour intervals (solid squares, triangles, and diamonds, pluses, and open diamonds, triangles, squares, and circles, respectively). Figure 2b plots only 0.5-m depth for highlighting soil moisture states in the top two layers.

Table 2. Experimental Setup

Case	Initial Soil Moisture in Each Layer						Updating Use	Integration Time	Infiltration at Surface
	First	Second	Third	Fourth	Fifth	Sixth			
1	0.122	0.122	0.122	0.122	0.122	0.122	Yes	48 hours	K_{sat} during whole time
2	0.122	0.122	0.122	0.122	0.122	0.122	No	48 hours	K_{sat} during whole time
3	0.122	0.122	0.122	0.122	0.122	0.122	Yes	96 hours	K_{sat} for the first 30 hrs
4	0.435	0.435	0.435	0.435	0.435	0.435	Yes	48 hours	no infiltration
5	0.435	0.435	0.435	0.122	0.122	0.122	Yes	48 hours	no infiltration
6	0.122	0.122	0.122	0.122	0.122	0.435	No	128 days	no infiltration

following rules [*Bonan*, 1996]: (1) Any soil water in excess of saturation is added back to the soil, starting at the top, to bring each successive soil layer to saturation. (2) Any remaining excess water is added to the subsurface drainage, requiring the condition $\theta \geq 0.01$ (mm^3/mm^3) by removing water from immediately lower layers to bring soil water to 0.01 mm^3/mm^3. The following tests show that this updating plays an important role in simulating the saturation flow in a dry soil.

The first series of experiments were designed to test the performance of the EWFAI assuming no evapotranspiration loss from the soil column during the simulation periods. Figure 2 shows the soil water profiles at the start and at 6-hour intervals. The corresponding initial and boundary conditions are given in Table 2.

Infiltration experiments were performed first with uniform soil moisture of 0.122 mm^3/mm^3. The boundary condition was defined by controlling the infiltration at a rate of K_s at the surface for the entire period. The results are shown in Figure 2a (designated as case 1). The EWFAI can simulate infiltration with a classic wetting front during the rainfall period (see also the loam infiltration panel of Figure 24 of *Bonan* [1996]). Case 2 is similar to case 1, except that the updating scheme is not used here. The results show that nearly all the infiltrated water stays at the top, and very little water enters the second layer. In case 3 the updating scheme is used again and infiltration is still controlled at the rate K_s, but only during the first 30 hours. The moisture profiles do not change after the 36th hour of simulation. Although soil moisture in the fourth layer is at saturation and the fifth layer is dry, no water infiltrates. Compared to case 1, cases 2 and 3 include the situation of a large moisture gradient between adjacent layers. In general, the drainage of soil moisture should continue after infiltration at the surface ceases, but this does not happen in the EWFAI simulations.

Cases 4, 5, and 6 in Figure 2 depict drainage under the assumptions of no water loss due to evaporation and no water infiltration from the top. In case 4 the soil moisture is initiated at saturation for the whole column. Drainage occurs throughout the whole column because the soil moisture gradients remain small (see also the loam drainage panel of Figure 24 of *Bonan* [1996]). The other two tests contain large gradients of soil moisture. In case 5, only the soil in the upper three layers is initiated at saturation, and the other layers are initiated dry with soil moisture of 0.122 mm^3/mm^3. The profiles remain the same throughout the entire simulation period of 48 hours, indicating no water movement. In case 6, which does not apply the updating rules, the soil in the bottom layer is kept at saturation and the other layers are initiated dry. Again, the presence of a sharp gradient causes the soil moisture profile to stay fixed throughout the total 128-day simulation.

In simulations from cases 2, 3, 5, and 6, large soil moisture gradients occur. As stated earlier, soil moisture in the NCAR-LSM (1.0) is modeled under the assumption of equal water flux on both sides of an interface. This approximation leads to the derivation of the transport coefficients at the interfaces. NCAR-LSM (1.0) uses equations (7) and (8) to describe moisture flux between two layers. (equation (8)) indicates that the coefficient K^* will be smaller or approximated as zero when the soil is very dry in one layer and wet in another. Thus there may be no water flux between the two layers (equation (8)) as was found in Figures 2b, 2c, 2e, and 2f. For example, the soils are at saturation in the fourth layer and dry in the fifth with a moisture value of 0.122 (mm^3/mm^3) in Figure 2c, and NCAR-LSM (1.0) fails to simulate drainage under these conditions. The reasonable results obtained in simulating saturation flow in a dry soil used the NCAR-LSM updating scheme (Figure 2a).

An error on soil moisture transport implies that climate will be modified because of sensitivity to soil moisture. For example, in NCAR-LSM (1.0), evapotranspiration (ET) is influenced by the soil moisture profile [*Bonan*, 1996] and may significantly contribute to land–atmosphere water exchanges [e.g., *Kelliher et al.*, 1993]. Therefore an accurate simulation of soil moisture is critical for modeling near-surface climate and land surface processes.

4. Soil Moisture and Latent Heat Comparisons

4.1. Benchmark Calculations

The Project for Intercomparison of Land-Surface Parameterization Schemes (PILPS) designed several numerical experiments to evaluate land surface schemes by first running models to equilibrium using observed atmospheric forcings, and then assessing their performance through comparison with field measurements [*Henderson-Sellers et al.*, 1993; *Shao and Henderson-Sellers*, 1996]. Here, we develop a criterion for evaluating the precision of hydrological modeling of NCAR-LSM (1.0) under existing and proposed transport coefficients.

All numerical schemes of soil hydrology in land surface models are designed to function at coarse spatial resolution and large time steps. NCAR-LSM uses six layers for the entire soil column of depth of 6.3 m. The solution of the differential equation (5), however, is best approximated by integration over a fine spatial grid and small time step [e.g., *Celia et al.*, 1990]. Therefore a set of experiments with very fine space and time steps were designed. The soil was divided

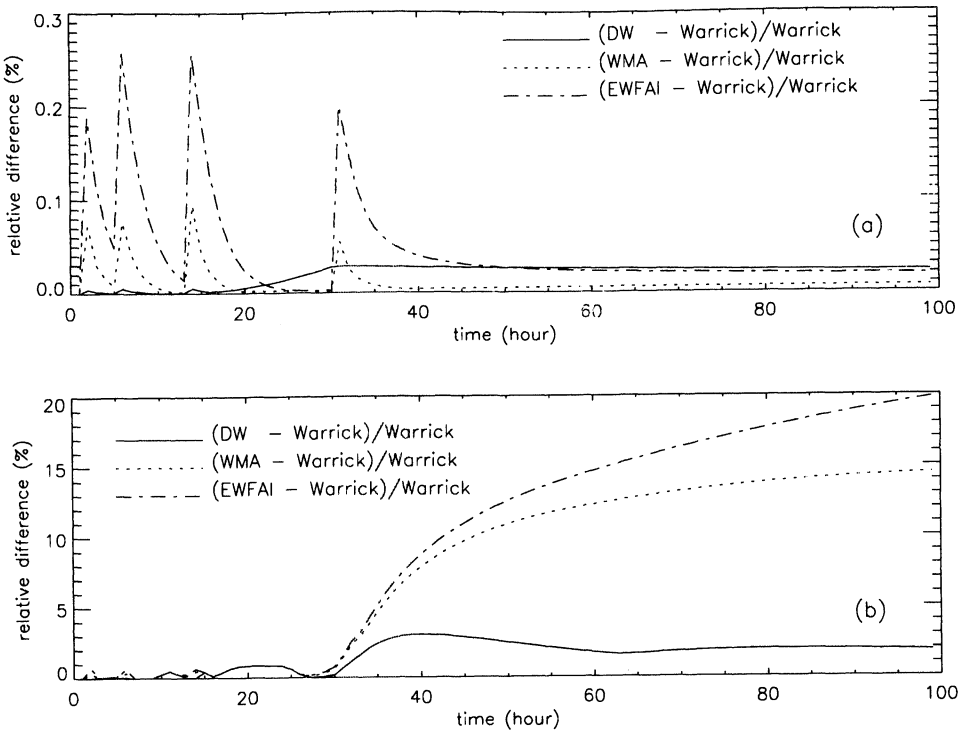

Figure 3. Relative difference of moisture defined in equation (20) for the entire soil column at (a) fine and (b) coarse resolutions. Solid lines show the relative difference between Dong and Wang's (DW) method and Warrick's method, dotted lines show the relative difference between the weighted moisture average (WMA) method and Warrick's method, and dashed lines are between the method of equal water flux across an interface (EWFAI) and Warrick's method. The profiles in Figure 3a are the relative difference obtained from lumped fine resolution at the scale of coarse-resolution.

into 630 layers of thickness 1 cm, and a 1-s time step was used. Initial soil moisture and boundary conditions were taken as case 3 discussed previously. The relative differences of the EWFAI [e.g., *Bonan*, 1996], the WMA method [e.g., *Foley*, 1996], and *Dong and Wang*'s [1997] method as compared to Warrick's method were calculated as

$$R_d = \frac{\sum_{i=1}^{nsl} \left| \theta_i^{(a)} - \theta_i^{(b)} \right| \Delta Z_i}{\sum_{i=1}^{nsl} \theta_i^{(b)} \Delta Z_i}. \quad (20)$$

In (20), $\theta_i^{(b)}$ is the averaged soil moisture in layer i at coarse resolution aggregated by Warrick's simulation under fine resolution, and $\theta_i^{(a)}$ is from one of the other three methods. The parameter nsl is the number of discretized soil layers (total of six layers) for coarse resolution. ΔZ_i is the thickness of soil layers. The relative differences between the different schemes are quite small (Figure 3a). The largest difference is between the EWFAI method and Warrick's method, but this is less than 0.3% and can be neglected. Under coarse resolution, $\theta_i^{(b)}$ is soil moisture in layer i from Warrick's simulation, and $\theta_i^{(a)}$ is again from one of the other three methods. However, the difference between these two methods can reach 19% at coarse resolutions (Figure 3b). The fine-resolution simulation results can be used as a benchmark to evaluate the precision of the various methods at coarse resolution.

4.2. Rainfall and Drainage Simulations

Two controlled experiments were designed to test four different numerical methods (EWFAI, WMA, *Warrick* [1991], and *Dong and Wang* [1997]) at coarse resolution. In one experiment the boundary condition was set with rainfall at rate K_s during the initial 30 hours, and in the other experiment another rainfall period from the 70th hour to the 80th hour was included. Both experiments assume no water loss due to evaporation, and the initial soil moisture is 0.122 (mm^3/mm^3) for the whole column. Results from the Warrick method at fine resolution were used as a benchmark to evaluate the other simulations. The relative difference in simulated soil moisture for the entire soil column between coarse resolution and fine resolution was defined as

$$\varepsilon_1 = \frac{\sum_{i=1}^{6} \left| \theta_i^{(a)} - \theta_i^{(b)} \right| \Delta Z_i}{\sum_{i=1}^{6} \theta_i^{(b)} \Delta Z_i}. \quad (21)$$

In (21), $\theta_i^{(a)}$ is soil moisture in layer i simulated by the various methods under coarse resolution. The value of $\theta_i^{(b)}$ is obtained by taking the average of soil moisture obtained under fine resolution to the corresponding layers in coarse spatial resolution. $\theta_i^{(b)} = \sum_{k=1}^{N(i)} w_k^{(b)} / N(i)$, where $w_k^{(b)}$ is the soil moisture in layer k of the fine-resolution grid, and $N(i)$ equals 10, 20, 40, 80, 160, and 320 from top to bottom of the coarse-resolution grid. ΔZ_i is the thickness of soil layers in coarse resolution. These two experiments were designed to test soil moisture simulation with rainfall and accompanying drainage (Figure 4). During the period of rainfall, all schemes result in small differences compared to the fine-resolution simulation (Figure 4a), in part because the updatings from NCAR-LSM (1.0) play an important role when simulating saturation flow

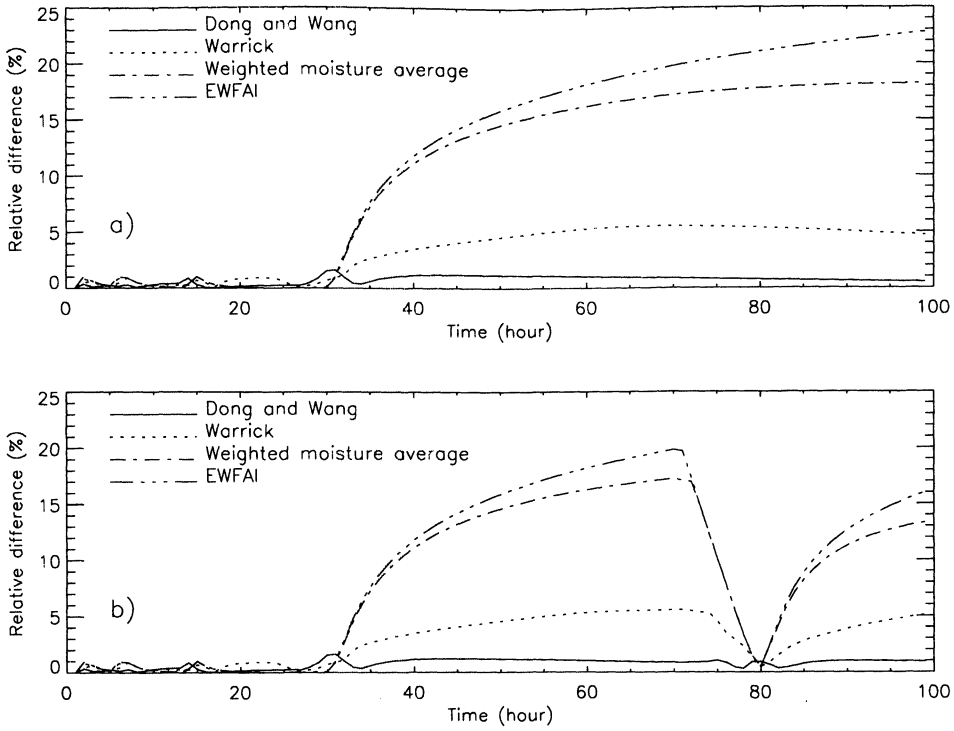

Figure 4. Relative difference between lumped fine-resolution (630 layers with time step of 1 s) and coarse resolution (six layers with time step of 10 min) simulations in soil moisture during rainfall and drainage. Results from the Warrick method under lumped fine resolution are used as reference to evaluate the other simulations. Rainfall is assumed (a) at the rate of saturated conductivity during the initial 30 hours and (b) including another rainfall event during the 70th hour to the 80th hour.

in a dry soil. However, during the drainage period, there are large differences in the simulated soil water movement. Warrick's and Dong and Wang's (W_DW's) methods result in small relative differences, typically less than 5%. The WMA and EWFAI methods result in 18% and 23% relative differences, respectively. Figure 4b indicates that rainfall can reduce the difference caused by drainage. However, after the rainfall the differences from the EWFAI and WMA methods increase quickly (16% and 14% at the 100th hour, respectively).

4.3. Evaporative Flux

Evaporation and transpiration combine to form the water vapor flux and thus the associated latent heat flux from the land surface to the atmosphere. To highlight the effect of soil moisture on evaporation and transpiration, another set of experiments are run with all parameters except soil moisture, leaf stomatal resistance, and surface resistance assumed constant. The evaporation in NCAR-LSM (1.0) is evaluated as

$$E_V = -\frac{\rho_{atm} C_p}{\gamma \lambda} \frac{e_{atm} - e^*(T_g)}{r_{aw} + r_{srf}}. \quad (22)$$

In (22), e_{atm} is the vapor pressure (pascals) at height z_{atm}, $e^*(T_g)$ is the saturation vapor pressure (pascals) at ground temperature, r_{aw} is the aerodynamic resistance (s/m) related to surface roughness, ρ_{atm} is air density (kg/m^3), and γ is the psychronmetric constant. The surface resistance r_{srf} is an

Table 3. Atmospheric Forcings and Land Surface Parameters

Term	Symbol	Value	Unit
Atmospheric pressure	P_{atm}	85351.4	Pa
Relative humidity	q_{atm}	10	g/kg
Temperature	T_{atm}	288.16	K
Wind speed	V_{atm}	1.0	ms^{-1}
Water content when ET ceases	θ_{dry}	0.122	mm^3 mm^{-3}
Optimal water content for ET	θ_{opt}	0.138	mm^3 mm^{-3}
Maximum rate of carboxylation at 25° C	V_{max25}	33	μmol m^{-2}s^{-1}
Snow cover	f_{snow}	0	dimensionless
Aerodynamic resistance	r_{aw}	10	s m^{-1}
Leaf area index	LAI	4.5	dimensionless
Stem area index	SAI	3.5	dimensionless
Leaf dimension	d_{leaf}	0.04	m
Cumulative root profile for grass	r_p	0.97	dimensionless

important variable linking evaporation with surface soil moisture and is expressed [*Bonan*, 1996] as

$$r_{srf} = 150 f_{sno} + (1 - f_{sno}) \frac{r_{aw}(1-\beta_e)}{\beta_e}. \quad (23)$$

In (23), β_e ranges from 1 when soil is wet to 0 when soil is dry through the linear equation $\beta_e=(\theta_1-\theta_{dry})/(\theta_{opt}-\theta_{dry})$. Other parameters are listed in Table 3. ET is defined [*Bonan*, 1996] as

$$E_{tr} = -\frac{\rho_{atm} C_p}{\gamma\lambda}[C_a^w e_{atm} + C_g^w e^*(T_g) - [C_a^w + C_g^w]e^*(T_v)]\frac{C_e^w + C_t^w}{C_a^w + C_e^w + C_t^w + C_g^w}. \quad (24)$$

In (24) the conductance C_t^w is defined as $(1-f_{wet})(L^{sun}/(r_b+r_s^{sun})+L^{sha}/(r_b+r_s^{sha}))$, and the definitions for other conductances (C_a^w, C_g^w, and C_e^w) are given by *Bonan* [1996]. The L^{sun} and L^{sha} are the sunlit and shaded leaf area indices and defined in section 3.1 of *Bonan* [1996], and the wetted fraction of canopy f_{wet} is set at 0 for testing transpiration from the leaf interior. The leaf boundary layer resistance r_b is a function of wind speed and vegetation height. The leaf stomatal resistance r_s, which links transpiration to soil moisture in the root zone through leaf photosynthesis, is used to calculate the conductance C_t^w and is defined by *Bonan* [1996]. In this simulation we take photosynthesis $A=0.5V_{max}$ for C_3 grass. The maximum rate of carboxylation V_{max} varies with temperature, foliage nitrogen, and soil water. The variable β_t, used to calculate V_{max}, is related to soil water through vegetation and is defined as $\beta_t=\Sigma W_i R_i$, where R_i is the relative root abundance and W_i is the available water in soil layer i. Similar to the variable β_e for the soil evaporation case, soil available water for transpiration in layer i can be expressed as $W_i=(\theta_i-\theta_{dry})/(\theta_{opt}-\theta_{dry})$. The relative root abundance R_i is modeled as $(1-r_p^z)$, where r_p is the cumulative root profile and z is soil depth.

In order to assess the influence of discretization discrepancies on ET, a relative difference in soil moisture can be defined as

$$\varepsilon_2 = \frac{\sum_{i=1}^{msl}\theta_i^{(a)}\Delta Z_i - \sum_{i=1}^{msl}\theta_i^{(b)}\Delta Z_i}{\sum_{i=1}^{msl}\theta_i^{(b)}\Delta Z_i}. \quad (25)$$

The term $\sum_{i=1}^{msl}\theta_i^{(a)}\Delta Z_i$ is the sum of soil water in the root zone from coarse spatial resolution simulations, and $\sum_{i=1}^{msl}\theta_i^{(b)}\Delta Z_i$ is the same sum from lumped fine-resolution simulations. The parameter ε_2 indicates the soil water difference in the root zone between the coarse and fine resolutions. To evaluate the feedback of simulated evaporation and transpiration on the soil water simulation, the corresponding relative error in cumulative ET is defined as

$$\varepsilon_{ET} = \frac{\sum_{t=1}^{T} ET_t^{(l)} - \sum_{t=1}^{T} ET_t^{(h)}}{\sum_{t=1}^{T} ET_t^{(h)}}. \quad (26)$$

Here $\sum_{t=1}^{T} ET_t^{(l)}$ and $\sum_{t=1}^{T} ET_t^{(h)}$ are the cumulative evaporation amounts at time T from coarse and fine spatial resolutions, respectively. The superscripts l and h represent the results obtained from the simulations in low (l) and high (h) resolutions.

The evaporation can be divided into at least two distinct stages for bare soil and in some cases vegetated surfaces. The first-stage evaporation rate is governed mainly by atmospheric conditions, and the second stage is limited by soil moisture.

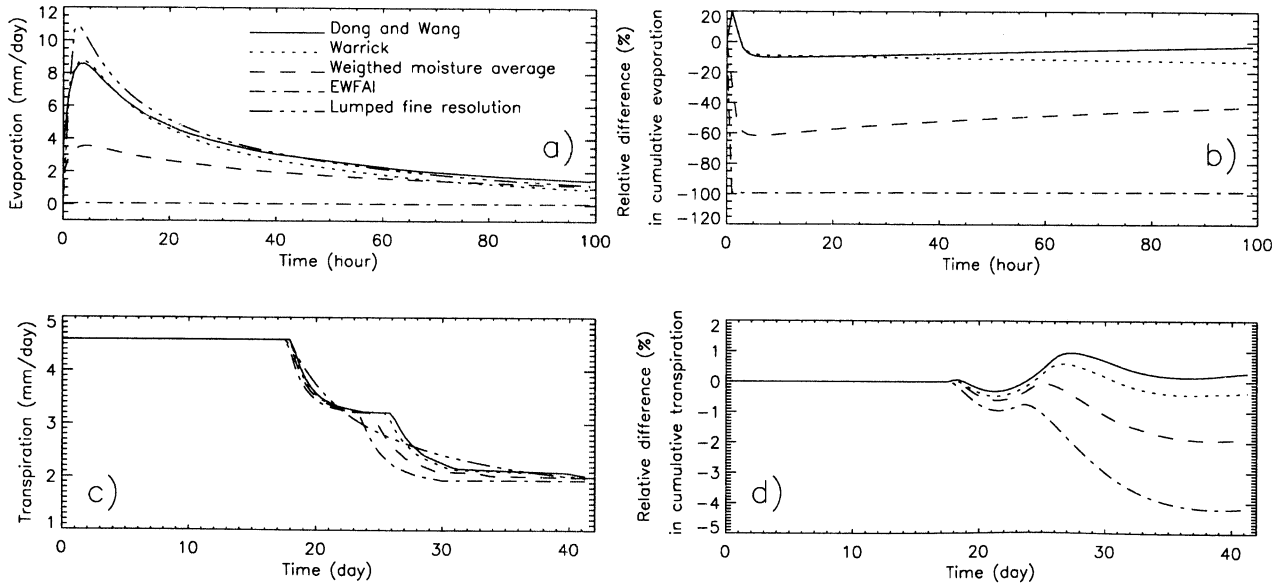

Figure 5. Simulations of evaporation and transpiration over a vegetated surface with the fixed atmospheric boundary conditions listed in Table 3. Relative difference in cumulative evaporation and transpiration is evaluated by equation (26), and the negative values show underestimation compared to the results from lumped fine resolution. The labels in Figures 5b-5d are the same as in Figure 5a.

During soil-limited evaporation the rate of evaporation is relatively independent of the soil surface layer humidity and may be estimated from equations based on soil moisture transport [*Philip*, 1957; see also *Salvucci*, 1997]. This experiment is designed to evaluate the response of the second-stage evaporation and transpiration to differences in the soil moisture profile caused by different numerical methods. For this purpose, soil moisture is initiated at a dry value of 0.122 (mm^3mm^{-3}) for the first layer and at 0.3 (mm^3mm^{-3}) for the other layers. Two kinds of land surface types are selected: a bare soil and a grass.

Figure 5 shows simulated evaporation and transpiration with fixed atmospheric boundary conditions (Table 3) by the four methods at coarse resolution, and then compared with results from the fine resolution. The results indicate that W_DW's methods simulate evaporation well, close to the simulated evaporation at fine resolution. The WMA method underestimates evaporation, and the EWFAI method simulates little evaporation during this period (Figures 5a). Water for evaporation is transported from the lower soil layers. The EWFAI simulates almost no evaporation because no water is available in the first layer. At the same time, no water can be transported to the first layer because of the model's inability to simulate water movement when large gradients of soil moisture are present. For W_DW's methods, the relative difference in cumulative evaporation is less than 10% when compared with the simulated results from the fine resolution. However, the relative difference remains 100% for the EWFAI case during the entire simulation, and is about 50% for the simulation using the WMA method (Figures 5b).

Similar to evaporation, transpiration over a vegetated surface can also be divided into two stages, limited by one of two factors: the potential transpiration rate or the soil moisture supply [*Denmeade and Shaw*, 1962]. Recent analytical and numerical modeling of water extraction by roots suggests that the duration of stage 1 transpiration depends on the storage capacity of the root zone, the potential transpiration rate, and the soil drainage and desorptive properties, while the stage 2 transpiration rate is controlled by the upward flux through the bottom of the root zone [*Levine and Salvucci*, 1999]. In order to test the impact of the above four numerical methods on the simulated transpiration during two stages, a long dry down period (42 days) is simulated with no water loss from evaporation at the surface. The resulting transpiration rate is the same for all four numerical methods under fine and coarse resolutions during approximately the first 18 days (Figure 5c). This result indicates that the soil is supplying enough water for transpiration during this period (first stage). There is no impact from the numerical methods during this stage. During the second stage, moisture storage for transpiration is transported from the soil layers below the root zone by capillary rise. W_DW's methods simulate 0.03% errors in cumulative transpiration at the end of integration. The relative errors using the WMA and EWFAI methods are 2% and 4%, respectively (Figure 5d). The EWFAI method underestimates transpiration amount again because of its inability to simulate the capillary rise under a large moisture gradient, as analyzed earlier in this section. Compared to the simulated evaporation, the impacts of numerical methods on transpiration are small.

5. Simulations With LSM Using Forcings From HAPEX

Atmospheric forcings from the HAPEX experiment at 30-min intervals [*Goutobe and Tarrieu*, 1991] were used to drive the LSM at a single spatial point. Measurements from June 1 to July 31 were used in this simulation. The atmospheric forcings are precipitation, temperature, solar radiation, longwave radiation, specific humidity, and wind speed. Precipitation and air temperature are shown in Figure 6. Solar radiation is partitioned into four components: (1) visible direct beam (35%), (2) near-infrared direct beam (35%), (3) visible diffuse beam (15%), and (4) near-infrared diffuse beam (15%). Four strong rainfall events occurred at the end of June, and the total precipitation was 333 mm during this period.

Bare soil (Figure 7) and warm grass (Figure 8) were considered with an initial soil moisture content of 0.3 mm^3mm^{-3}. During the period of simulation, infiltration calculated by the different methods was set equal to precipitation (Figure 7a). Therefore all precipitation infiltrates into the soil and no water joins surface runoff. The cumulative evaporation totals calculated by the *Dong and Wang* [1997] and *Warrick* [1991] methods under low (six layers) resolution are nearly the same as calculated from the fine-resolution simulations. The EWFAI simulates 30 mm less evaporation than that calculated from fine resolution (Figure 7c). This

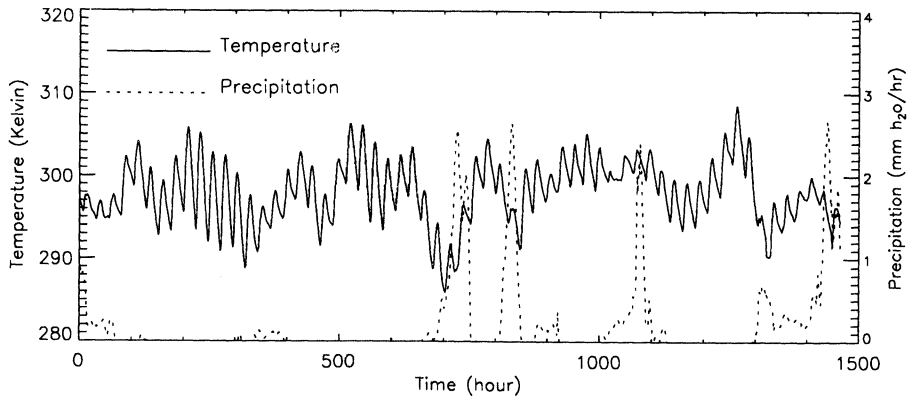

Figure 6. The Hydrologic Atmospheric Pilot Experiment (HAPEX) precipitation and temperature at a 30-min interval from June 1 to July 31. These data, combined with solar wave radiation, longwave radiation, specific humidity, and wind speed, will be used as atmospheric forcings to drive off-line LSM simulations.

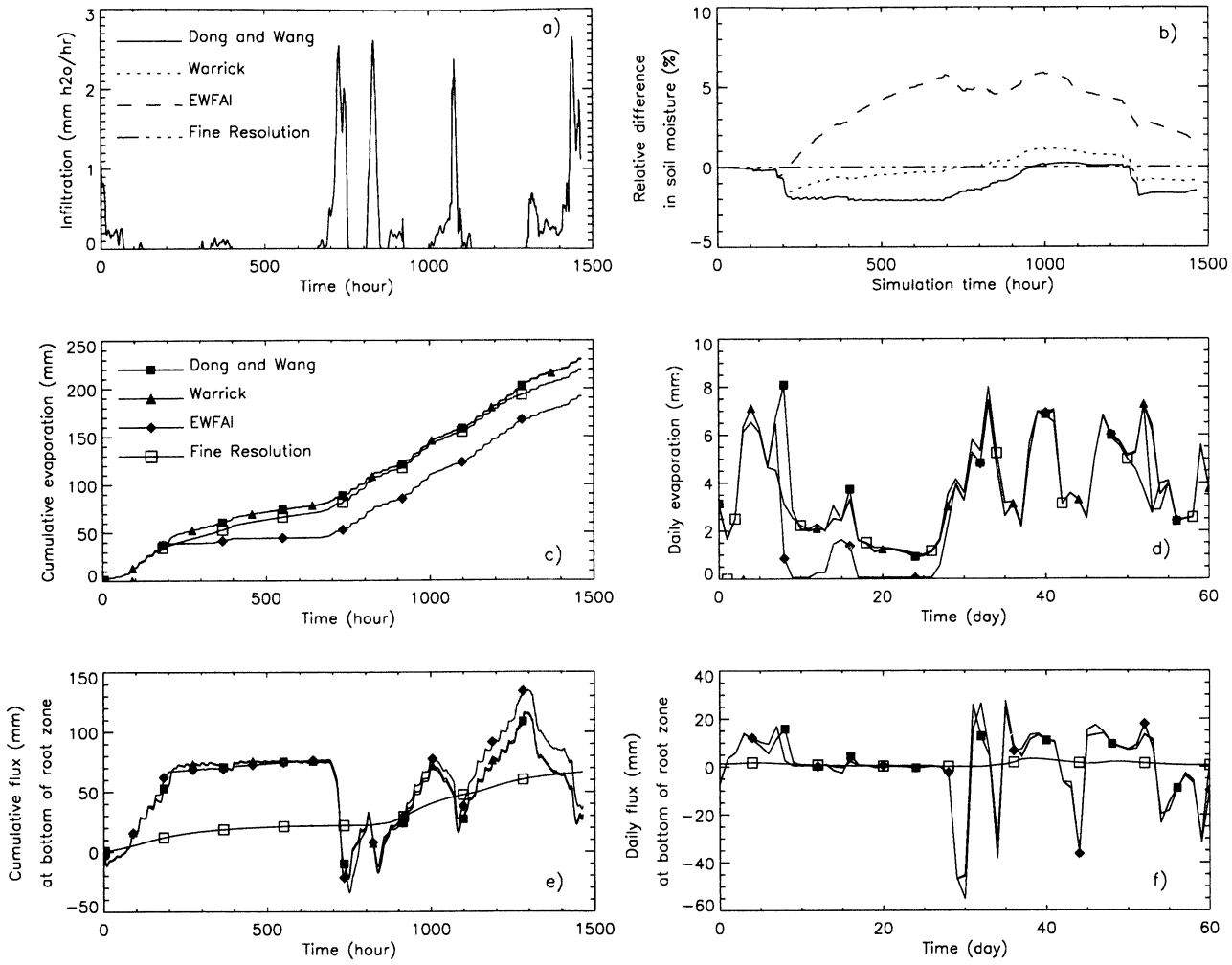

Figure 7. Simulation with the off-line LSM forced by the HAPEX atmospheric data set for a bare soil. Cumulative and daily water fluxes are evaluated at 1.5 m, and the positive values are displayed in the upward direction. The infiltration is simulated the same for all four methods (see Figure 7a). The labels for Figure 7b are the same as those for Figure 7a, and those for Figures 7d-7f are the same as for Figure 7c. Relative difference in soil moisture (Figure 7b) is evaluated by equation (25).

underestimation begins at about the 200th hour and lasts from day 8 to day 26 (Figure 7d). During the rainfall period, there were small differences in soil evaporation rates because sufficient water was available near the soil surface. However, as the surface soil dries quickly, the EWFAI method cannot simulate the flux of water from the second layer to the first layer because of the large moisture gradients present. This causes an underestimation of evaporation.

Figure 8 shows the simulated results for a warm grass land cover. The EWFAI method again underestimates the flux to the atmosphere, this time by 20 mm compared to the other methods. This flux mostly comes from surface soil evaporation rather than transpiration (Figures 8a, 8c, and 8d). This underestimation of evaporation during days 16-28 is also caused by the dry first layer and lack of water supply from the lower layers (Figure 8b).

The soil in the top 1.5-m depth contains 99% of the root biomass in the case of the warm grass. The moisture flux at this depth is analyzed to determine the difference in the simulation of soil moisture drainage (relative difference for the bare soil case as well). The cumulative flux curve at the bottom of the root zone simulated with the fine-resolution method varies smoothly (Figures 7e and 8e). The flux simulation at coarse resolution fluctuates strongly (Figures 7e and 8e), especially during the July rainfall period when the flux is downward at 50 mm per day on the 30th day, and then upward at 30 mm per day by the 35th day (Figure 7f). The difference in drainage simulation between the coarse and fine resolutions is mainly due to differences in spatial resolution and is not related to the different methods of estimating transport coefficients.

The relative difference in soil moisture simulated by the EWFAI method reaches 6% for the bare soil and the warm grass, while the W_DW methods simulate soil moisture with less than 2% relative difference (Figures 7b and 8f). As discussed above, the discrepancy is due partly to evaporation and partly to drainage. Compared to drainage, the differences from evaporation in simulating soil moisture movement are small. Evaporation, however, is an irreversible process in the soil water budget, while a fraction of drained water may later be lifted back into the root zone by capillary rise [e.g., *Levine and Salvucci*, 1999]. In June, all three methods simulate

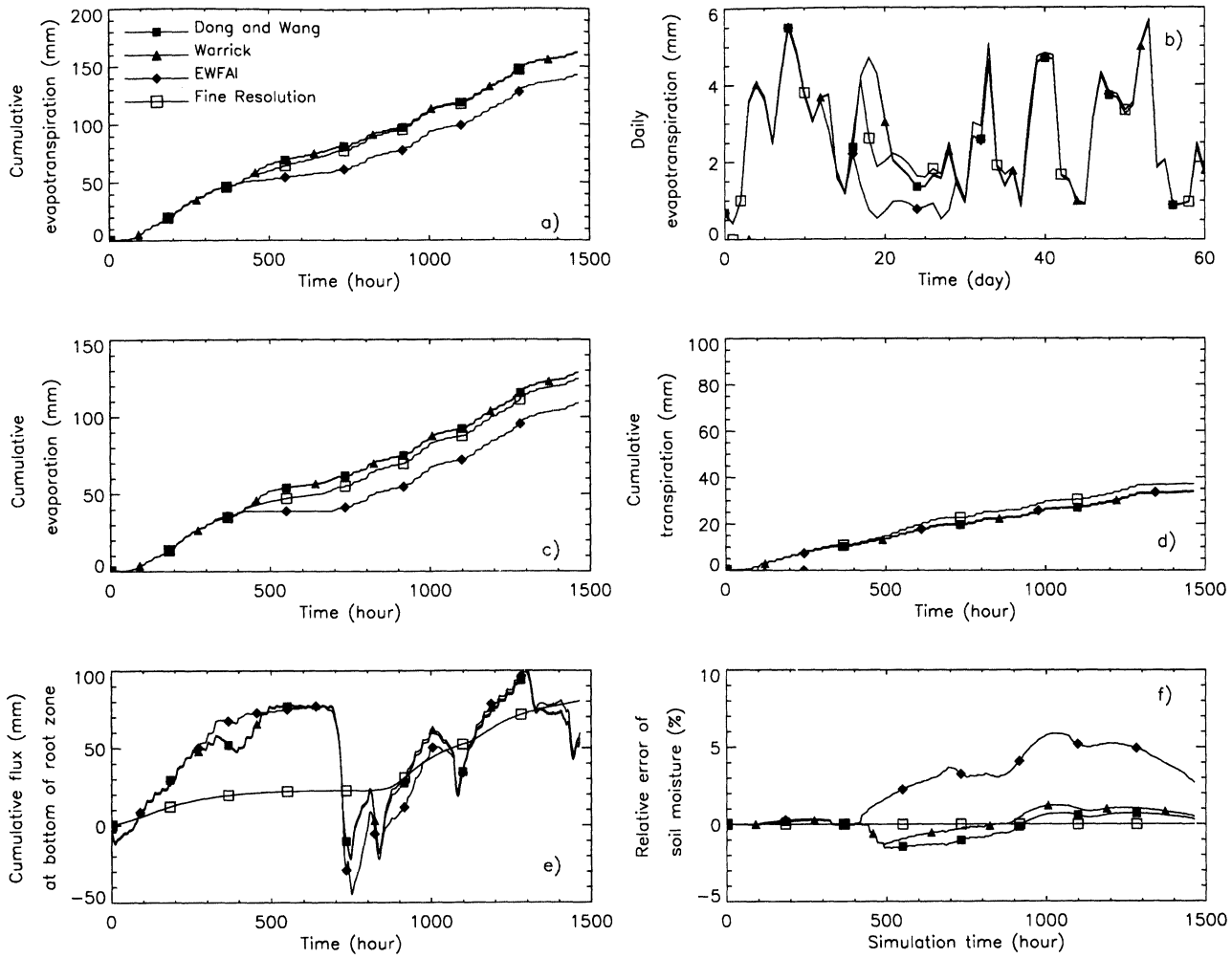

Figure 8. Simulation with the LSM forced by HAPEX data in the case of a warm grass land cover. Cumulative and daily fluxes are evaluated at 1.5 m, and the positive values are in the upward direction. The cumulative evapotranspiration (Figure 8a) is separated into evaporation (Figure 8c) and transpiration (Figure 8d) to identify the error sources. The daily evapotranspiration (Figure 8b) illustrates the difference occurring during days 16-28 after a long dry period. Relative difference in soil moisture (Figure 8f) is evaluated by equation (25).

nearly the same upward flux at coarse resolution, and higher upward flux at the bottom of the root zone leads to more soil water in the root zone. However, soil water content is underestimated, as shown in W_DW's simulations (Figures 7e and 7b for a bare soil case, and Figures 8e and 8f for a vegetated case). In this case, evaporation is the source of the discrepancy in the W_DW simulations, and higher upward flux is simulated to reduce some of the differences caused by evaporation. In the case of the EWFAI, the relative difference in soil moisture is partly due to the underestimation of evaporation and partly due to higher upward flux (Figures 7b and 7d).

6. Conclusions and Discussion

On the basis of the above numerical experiments, it appears that the following conclusions can be made:

1. As has been demonstrated by others, the simulation of water movement through soil depends on the performance of numerical methods, especially at coarse resolution and in the presence of sharp moisture gradients. The unsaturated flux simulations with the assumption of equal water flux across an interface (e.g., NCAR-LSM (1.0)) and the method of weighted moisture average (e.g., IBIS of Foley et al. [1996]) lead to large discrepancies compared to fine-resolution simulations. For example, the difference in simulated soil moisture from the EWFAI and WMA methods increases quickly during a drainage period after a heavy rain of short duration over a dry soil.

2. The simulated stage-2 soil evaporation, but not transpiration, is sensitive to the choice of numerical schemes for the simulation of moisture transport. The discrepancies are especially evident in evaporation during long dry seasons. Such differences are again caused by a sharp gradient of soil moisture. W_DW's methods for estimating effective transport coefficients can handle such gradients and thus simulate similar evaporation totals under fine and coarse resolutions.

3. Because the evaporated water cannot reenter the soil root zone to offset the simulated effects from former time steps during the dry season, the discrepancy in soil moisture in the case of W_DW's methods is due to evaporation simulation. In the case of the EWFAI method, the bias is partly due to

evaporation with the same magnitude compared to W_DW's methods and partly due to simulated soil moisture transport. The simulation of soil water transport in W_DW's methods can reduce some of the differences caused by evaporation simulations. The EWFAI method has this capability only during rainfall events. Without rainfall the simulated soil moisture transport cannot reduce and may actually increase the errors in soil moisture. Finally, W_DW's methods display smaller differences in hydrologic flux simulations between fine and coarse resolutions than the EWFAI method.

Soil moisture movement in the unsaturated zone provides a critical coupling between the atmospheric and subsurface branches of the hydrologic cycle, and the response of the unsaturated zone to varying atmospheric forcings strongly affects the energy budget at the soil-atmosphere interface, and thus soil hydrological simulation plays an important role in climate models. Various numerical experiments suggest that soil moisture anomalies can persist long enough to change the atmospheric circulation over seasonal to interannual timescales [e.g., *Yeh et al.* 1984; *Serafini*, 1990]. Since numerical schemes can result in large differences in the simulation of water flux under coarse spatial resolution, they can also affect the simulated near-surface climate.

For example, the coupled atmosphere (CCM3) and land (LSM) models driven by observed sea surface temperature (SST) for the period December 1978 to September 1993 simulated pronounced cold biases in the Northern Hemisphere [*Bonan*, 1998]. The biases were attributed to overly wet soil simulated from the land model. As seen above, the EWFAI method for the simulation of soil moisture transport in NCAR-LSM (1.0) cannot simulate continued drainage after a short heavy rainfall event. It is possible that a simple modification of the simulation of soil water transport using *Dong and Wang*'s [1997] method for estimating transport coefficients could correct such biases in simulated climate. This could be very simply accomplished by replacing equations (7) and (8) in LSM with equations (17), (18), and (19). Future research will address the feedback of climate-modeled temperature and precipitation to numerical simulation techniques.

Acknowledgments. We thank the NCAR community for making available CCM and LSM to the public. This work was funded by NOAA/NASA grant NA76GP0481.

References

Bonan, G. B., Hydrology: A land surface model (LSM version 1.0) for ecological, hydrological, and atmospheric studies: Technical description and user's guide, *NCAR Tech. Note, NCAR/TN-417+STR*, 88-102, 1996.

Bonan, G. B., The land surface climatology of the NCAR land surface model coupled to the NCAR Community Climate Model, *J. Clim.*, *11*, 1307-1326, 1998.

Celia, M.A., F.T. Bouloutas, and R.L. Zarba, A general mass-conservative numerical solution for the unsaturated flow equation, *Water Resour. Res.*, *26*, 1483-1496, 1990.

Clapp, R.B., and G.M. Hornberger, Empirical equations for some soil hydraulic properties, *Water Resour. Res.*, *14*, 601-604, 1978.

Cosby, B. J., G. M. Hornberger, R. B. Clapp, and T. R. Ginn, A statistical exploration of the relationships of soil moisture characteristics to the physical properties of soils, *Water Resour. Res.*, *20*, 682-690, 1984.

Denmeade, O.T., and R.H. Shaw, Availability of soil water to plants as affected by soil moisture and meteorological conditions, *Agron. J.*, *54*, 385-429, 1962.

Dickinson, R. E., A. Henderson-Sellers, P. J. Kennedy, and M. F. Wilson, Biosphere-Atmosphere Transfer Scheme (BATS) for the NCAR Community Climate Model, *NCAR Tech. Note, TN-275+STR*, 72 pp., 1986.

Dong, J., and A.S. Wang, The difference scheme of soil hydraulic conductivity and diffusivity and experimental tests, *Prog Nat. Sci.*, *7*(6), 707-714, 1997.

Foley, J. A., I. C. Prentice, N. Remankutty, S. Levis, D. Pollard, S. Sitch, and A. Haxeltine, An integrated biosphere model of land surface processes, terrestrial carbon balance, and vegetation dynamics, *Global Biogeochem. Cycles, 10*(4), 603-628, 1996.

Goutobe, J. P., and C. Tarrieu, HAPEX-MOBILHY database, in Land Surface Evaporation, edited by T.J. Schmugge and J.C. Andre, pp. 403-410, Springer-Verlag, New York, 1991.

Haverkamp, R., M. Vauclin, J. Touma, P. J. Wierenga, and G. Vachaud, A comparison of numerical simulation models for one-dimensional infiltration, *Soil Sci. Soc. Am. J.*, *41*, 285-294, 1977.

Haxeltine, A., and I. C. Prentice, BIOME3: An equilibrium terrestrial biosphere model based on ecophysiological constraints, resource availability, and competition among plant types, *Global Biogeochem. Cycles, 10*(4), 693-709, 1996.

Henderson-Sellers, A., Z.L. Yang, and R.E. Dickinson, The Project for Intercomparison of Landsurface Parameterization Schemes (PILPS): Phase 2 & 3, *Bull. Am. Meteorol. Soc.*, *76*, 489-503, 1993.

Hillel, D., *Fundamentals of Soil Physics*, Academic, San Diego, Calif., 1980.

Kelliher, F.M., R. Leuning, and E.D. Schulze, Evaporation and canopy characteristics of coniferous forest and grasslands, *Oecologia, 95*, 153-163, 1993.

Kutilek, M., and D.R. Nielsen, Darcy-Buckingham equation, in *Soil Hydrology, GeoEcology Textbook*, pp. 87-119, Catena, Reiskirchen, Germany, 1994.

Levine, J.B., and G.D. Salvucci, Characteristic rate scale and timescale of supply-limited transpiration under a Richards-Cowan framework, *Water Resour. Res.*, *35*, 3947-3954, 1999.

Philip, J.R., Evaporation and moisture and heat fields in the soil, *J. Meteorol.*, *14*, 354-366, 1957.

Salvucci, G.D., Soil and moisture independent estimation of stage-two evaporation from potential evaporation and albedo or surface temperature, *Water Resour. Res.*, *33*, 111-122, 1997.

Sellers, P. J., Y. Mintz, Y. C. Sud, and A. Dalcher, A simple biosphere model (SiB) for use within general circulation models, *J. Atmos. Sci.*, *43*, 505-531, 1986.

Serafini, Y.V., The time scale of land surface hydrology in response to initial soil moisture anomalies: A case study, *Tellus, 42A*, 390-400, 1990.

Shao, Y., and A. Henderson-Sellers, Modelling soil moisture: A project for Intercomparison of Land Surface Parameterization Schemes Phase 2(b), *J. Geophys. Res.*, *101*, 7227-7250, 1996.

Warrick, A. W., Numerical approximations of Darcian flow through unsaturated soil, *Water Resour. Res.*, *27*, 1215-1222, 1991.

Yeh, T.C., R.T. Wetherald, and S. Manabe, The effect of soil moisture on the short-term climate and hydrology change: Numerical experiment, *Mon. Weather Rev.*, *112*, 474-490, 1984.

J. Dong, G. D. Salvucci, and R. B. Myneni, 675 Commonwealth Avenue, Department of Geography, Boston University, Boston, MA 02215-1406. (jjrdong@bu.edu)

(Received May 31, 2000; revised November 29, 2000; accepted January 30, 2001.)